Autonomous Assistance-as-Needed Control of a Lower Limb Exoskeleton With Guaranteed Stability

SAMUEL M. CAMPBELL[1], **CHRIS P. DIDUCH**[2], **(Senior Member, IEEE),**
AND JONATHON W. SENSINGER[1,2], **(Senior Member, IEEE)**
[1]Institute of Biomedical Engineering, University of New Brunswick, Fredericton, NB E3B 5A3, Canada
[2]Department of Electrical and Computer Engineering, University of New Brunswick, Fredericton, NB E3B 5A3, Canada

Corresponding author: Samuel M. Campbell (scampbe5@unb.ca)

ABSTRACT The use of exoskeletons for clinical lower-limb stroke rehabilitation offers the potential of improved and customized rehabilitation that reduces the requirements and demands placed on multiple staff members. Initial research with lower-limb exoskeletons show potential to alleviate this problem. Conventional assistance-based exoskeleton devices simply enforce the desired gait trajectory for the patient in order to ensure safety and stability. Unfortunately, if the end-user does not have to work to contribute to successful motion, rehabilitation often does not occur. Recent evidence has suggested that assistance-as-needed control prevents users from slacking, facilitating functional motor recovery. Assistance-as-needed control turns off assistive torques during periods when the patient is able to execute a desired gait pattern but if the patients gait deviates sufficiently from a desired trajectory then assistive torques are generated to compensate for the patients loss of strength. This strategy encourages the patient to contribute effort while still enabling the exoskeleton to guide movements. Assistance-as-needed control inherently leads to aperiodic gait patterns and has accordingly been difficult to employ in lower-limb exoskeletons due to the need to ensure stability. This work demonstrates how virtual constraint control—a method with robust stability properties used in prostheses and assistive exoskeletons control—can be combined with a velocity-modulated deadzone to ensure stability. Simulations suggest that the method can accommodate a large deadzone while remaining stable across a range of unanticipated gait pathologies, as demonstrated using Lorenz mappings that can accommodate the aperiodic nature of the resulting gait.

INDEX TERMS Exoskeletons, bipedal gait, rehabilitation, assistance-as-needed, stability, virtual constraints.

I. INTRODUCTION

Each year, approximately 15 million people suffer from a stroke worldwide and 5 million of these individuals are left with a permanent disability [1]. Current stroke rehabilitation practices are physically demanding and require the effort of multiple physiotherapists. Researchers are accordingly investigating the use of lower limb electromechanical exoskeletons as a means to facilitate gait rehabilitation [2]. Many exoskeleton devices simply perform the desired gait trajectory for the individual in order to ensure safety and stability [3]–[5].

The associate editor coordinating the review of this manuscript and approving it for publication was Wangli He.

Unfortunately, if the exoskeleton ensures the correct trajectory regardless of whether or not the user contributes effort, it can result in an unsuccessful rehabilitation process as the patient can become reliant on the device and begin to slack in their rehabilitation training program [6].

The central aim of our work is to design a lower-limb exoskeleton control strategy that promotes functional rehabilitation following a stroke by preventing the user from slacking. In order to properly rehabilitate someone who has had a stroke, one must promote brain plasticity and functional motor recovery. Brain plasticity is the functional reorganization or creation of neural connections in the brain that allow for the learning of a task following a brain injury [7].

There are many facets of neurological rehabilitation that can be studied and incorporated into an exoskeleton control strategy that best promotes brain plasticity and functional motor recovery [7]. Recent exoskeleton models are starting to converge on the idea of assistance-as-needed (AAN) control as a means to facilitate functional motor recovery by preventing slacking. Assistance-as-needed control ensures the patient puts forth maximum effort in the completion of their gait by applying the required compensatory torques to account for the patient's weakness.

Early adopters of the AAN control framework created control strategies that allow for a manual reduction in the amount of assistance provided to the user limbs [8]–[11]. This manual reduction in assistance requires active therapist tuning to best accommodate the patient's changing level of disability.

More complex AAN control strategies remain passive as long as the patient is on track in their gait cycle, but if they deviate too far from the desired trajectory, then the controller provides the required torques to compensate for the patient's weakness. This compensatory torque attempts to ensure that the patient completes a biomimetic walking pattern while encouraging them to contribute effort. The work done in [12] presents an example of an adaptive AAN policy using an end effector tunnel around the desired trajectory as a means to actively provide the proper assistance torques throughout the gait cycle without therapist specific tuning.

Advances in non-linear control theory have led to the development of more sophisticated control techniques and stability analyses that can address the needs of AAN rehabilitative control strategies. One such technique is an autonomous control strategy called virtual constraint control, which uses a phase variable to enforce virtual constraints, ensuring stability via a set of hybrid zero dynamics [13], [14]. Virtual constraint control has been implemented on lower limb prosthetics [15] and assistive lower-limb exoskeletons [5] with demonstrated robust stability properties. In this work we apply virtual constraints to a rehabilitative exoskeleton to create an autonomous control framework with demonstrated stability properties.

In order to validate the proposed controller, a dynamic model was created to simulate a combined human-exoskeleton system with 6 degrees of freedom of actuation in the sagittal plane. The Lagrangian dynamic model accurately represents the different phases of gait present in typical human locomotion, including non-instantaneous double support phase, fully actuated swing and stance phase, and an underactuated phase during terminal stance. The model provides an accurate representation of human walking despite its simple structure by combining the work done in [16] and [17]. Model validation is shown in Section II of this paper.

In Section III, the implementation of virtual constraint control as a means to enforce an autonomous control framework is described. Section IV describes the design of the assistance-as-needed control policy. The control policy ensures that there is active consideration of the patient's

retained strength throughout the completion of their gait rehabilitation.

Conventional virtual constraint control cannot guarantee stable trajectories in the presence of the large deadzones that are required to implement clinically realistic assistance-as-needed rehabilitation. The key innovation of this paper, described in Section V, is to incorporate a velocity constraint on the size of the deadzone that ensures momentum conservation and stability.

Simulation results and stability analyses are presented and discussed in Section VI for different gait pathologies, one of which is commonly developed following a stroke. In particular, we analyzed stability using Lorenz mappings rather than Poincare mappings as this allows for the analysis of aperiodic systems. The autonomous AAN control policy is aperiodic given the lack of a dependence on time or strictly enforced joint angle trajectories, thus allowing for variations in positional and velocity state information on a step to step basis. Finally, Section VII gives concluding thoughts and proposes future work.

II. DYNAMIC MODEL FORMULATION

In order to properly capture the dynamics associated with human walking, a model was created with three sub-phases. These sub-phases include the fully actuated swing and stance phase, as well as the non-instantaneous double support phase and the underactuated phase of gait that occurs during terminal stance. Coupling these three gait phase models led to a simulation that captured all of the kinematics and dynamics associated with human walking (see Figure 1). The masses associated with each of the links of the biped as well as the total mass of the model can be seen in Table 1.
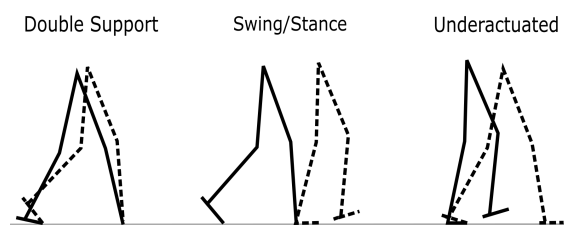

FIGURE 1. Phases of gait associated with the dynamic model. Within each phase the beginning position of the model is depicted in solid lines and it progresses to the ending position, depicted in dashed lines. When one phase of gait ends, the next begins meaning that there are no unmodelled aspects of the gait cycle.

A. CHOOSING A SIMPLIFIED MODEL

In the fully actuated phases of gait, the dynamic model was simplified by reducing the number of links included in the Lagrangian formulation from seven links to six links. This reduction in modelling complexity used the technique outlined in [16], which models the stance foot as a point torque at the heel joint thus eliminating the need to model the stance foot link in the fully actuated phases of gait (see Figure 2).

The fully actuated phases of gait include the majority of the swing/stance phase as well as the double support phase.

TABLE 1. Link masses associated with the dynamic model.

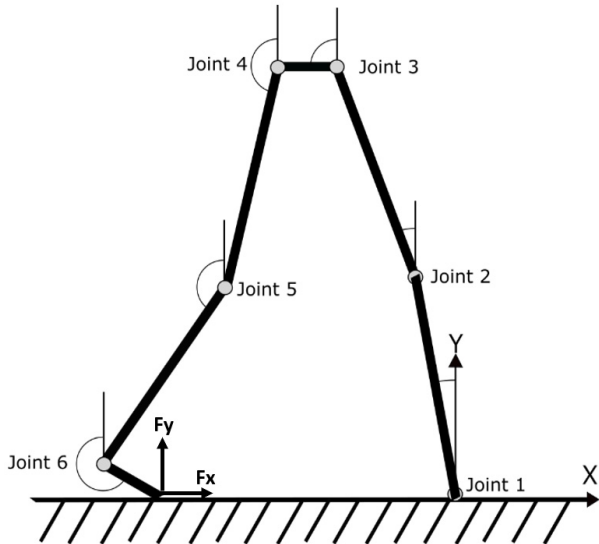| Links (Swing and Stance Leg)	Mass (kg)
Foot Link	1.12kg
Knee Link	3.72kg
Hip Link	8.23kg
Torso Link	43.20kg
Total Mass	**78.4kg**

FIGURE 2. The kinematic model used to formulate the biped's dynamics. The stance foot is replaced with a control torque at Joint 1 simplifying the Lagrangian modelling.

Modelling the stance foot as a point torque reduces the dimension of the dynamics from a seven degree of freedom (DoF) bipedal walker to a six DoF bipedal walker without a loss in modelling accuracy. The model is given by,

$$B_{(6 \times 6)} \ddot{\theta}_{i(6 \times 1)} = C_{(6 \times 1)} + (M_{i+1} - M_i)_{6 \times 1}, \quad (1)$$

where $1 < i < 6$ is representing each of the actuated degrees of freedom, $\ddot{\theta}_{(6 \times 1)}$ is the joint angular accelerations, $M_{i+1} - M_i$ is the total moment applied to each of the links, $B_{(6 \times 6)}$ is the inertial matrix, and $C_{(6 \times 1)}$ is a combination of Coriolis and gravitational terms. Representing the stance foot dynamics as a point torque also avoids singularities when attempting to determine the magnitude and location of the ground reaction force on the stance foot.

The second technique used to reduce the complexity of the dynamic model, presented in [17], eliminates the need for branch chain modelling of the torso by representing the center of mass (CoM) of each link with an additional eccentric component (see Figure 3). Although the eccentric component of the CoM is irrelevant for most of the joints, it becomes crucial in the formulation of the torso dynamics. The torso dynamics are included by modelling the link connecting the stance hip joint to the swing hip joint as having a length of
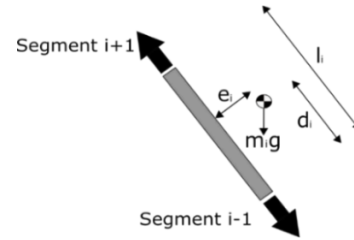
FIGURE 3. The CoM representation for each link in the kinematic chain, as per [17]. By including a non-zero eccentricity at the link connecting the stance hip joint to the swing hip joint of the biped, the dynamic effect of the unmodelled torso link is modeled without the need for branch chain modelling.

zero with an eccentric CoM in the sagittal plane. This non-zero eccentricity includes the torso in the dynamics without requiring a branch chain to model it.

B. NON-INSTANTANEOUS DOUBLE SUPPORT

The double support phase is often treated as instantaneous in a simulation framework to simplify calculations [14], [18]–[21]. As a result, roughly 20% of healthy human walking goes unmodelled and can not be considered in the analysis of proposed control policies. Achieving the non-instantaneous double support phase of gait is done by constraining the motion of the trailing foot link of the fully actuated model such that the toe remains on the ground until the biped moves into the swing phase [17]. Two constraint equations are used,

$$f_1 = \left(\sum_{i=1}^{n} (-l_i sin(\theta_i)) \right) + S = 0 \quad \text{(horizontal)} \quad (2)$$

$$f_2 = \left(\sum_{i=1}^{n} (l_i cos(\theta_i)) \right) = 0 \quad \text{(verticle)} \quad (3)$$

where l_i is the link length, θ_i is the joint angle with respect to vertical, S is the step length, f_1 is the constraint ensuring step length remains the same, and f_2 is the constraint ensuring the foot remains on the ground. The two constraints must be satisfied to ensure the biped achieves rotation about the trailing toe. Given the constraints in equations 2 and 3, the dependent joint angle trajectories can be computed to ensure the constraints are satisfied. In the case of this bipedal walker, the dependant angles were chosen to be the trailing legs knee and ankle joint.

Defferentiating the constraint equations twice allows for the constraint forces ($\lambda_{f1}, \lambda_{f2}$) on the trailing toe to be determined to ensure toe remains in contact with the ground throughout the double support phase [17]. The constraint force equations are added to the formulation of the dynamics, thus ensuring that they are actively considered throughout double support:

$$\begin{bmatrix} B_{(6 \times 6)} & l_i cos(\theta_i)_{6 \times 1} & l_i sin(\theta_i)_{6 \times 1} \\ l_i cos(\theta_i)_{1 \times 6} & 0 & 0 \\ l_i sin(\theta_i)_{1 \times 6} & 0 & 0 \end{bmatrix} \begin{bmatrix} \ddot{\theta}_{i6 \times 1} \\ \lambda_{f1} \\ \lambda_{f2} \end{bmatrix}$$

$$= \begin{bmatrix} C_{(6 \times 1)} \\ \sum_{i=1}^{6} l_i \dot{\theta}_i sin(\theta_i) \\ \sum_{i=1}^{6} -l_i \dot{\theta}_i cos(\theta_i) \end{bmatrix} + \begin{bmatrix} (M_{i+1} - M_i)_{6 \times 1} \\ 0 \\ 0 \end{bmatrix} \quad (4)$$

where the only previously undefined term $\dot{\theta}_i$, is the link angular velocity

The double support phase now becomes an 8×8 system of equations due to the two added Lagrangian constraint force calculations representing estimates of the horizontal and vertical ground reaction forces on the trailing toe. During this constrained double support phase of gait, the dynamics associated with the model are still 6 DoF. No longer modelling the double support phase as instantaneous means the dynamics within this phase can now be analyzed, thus resulting in a more accurate representation of human gait.

C. UNDERACTUATED PHASE
The underactuated phase of gait is triggered when the CoM of the bipedal model projected onto the ground passes over the stance toe thus causing rotation about this joint. This rotation about the stance foot means the stance foot must now be included in the formulation of the dynamics and cannot be modelled as simply a control torque at the heel. Adding the stance foot into the dynamic model formulation results in a 7 DOF system:

$$B_{(7 \times 7)} \ddot{\theta}_{i(7 \times 1)} = C_{(7 \times 1)} + (M_{i+1} - M_i)_{7 \times 1} \quad (5)$$

This phase of gait is considered to be underactuated as there is an inability to apply torque at the stance toe when the biped begins to rotate, hence tracking of a desired trajectory at this joint cannot be achieved. Through the implementation of an underactuated phase on a model with feet a more accurate representation of human walking in the sagittal plane is achieved. This accurate yet simplified model of human walking is used as the testbed to simulate the proposed control framework.

III. VIRTUAL CONSTRAINT IMPLEMENTATION
A common limitation of current rehabilitation exoskeleton controllers is that although they are able to replicate biomimetic gait, stability is very difficult to guarantee. The difficulty in guaranteeing stability stems from the fact that time-dependent joint angle trajectories are used as references for the controller. Not guaranteeing stability means that the exoskeleton can only be used at slow speeds, in regulated environments, and with the use of external stability aids such as crutches or a walker.

Current advances in non-linear control now allow for these reference trajectories to become autonomous using a technique known as virtual holonomic constraints [13], [22]. This reference trajectory generation technique replaces time with another monotonically increasing variable known as a phase variable (see Figure 4). In this work, the phase variable was chosen to be the angle created between the stance ankle of the
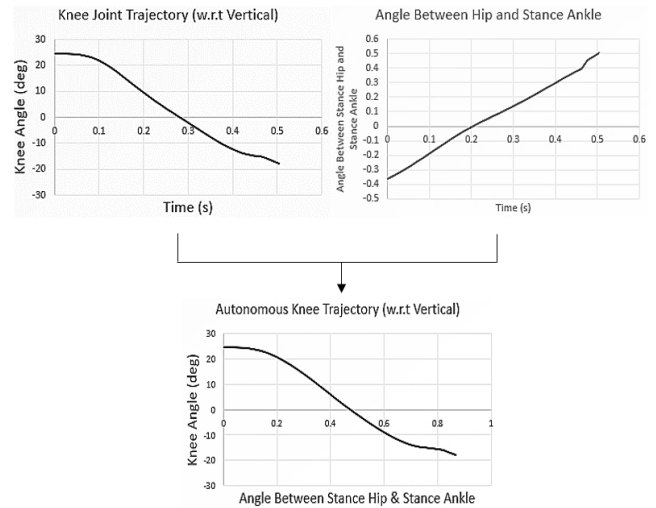

FIGURE 4. The example of the virtual constraint formulation shows that the dependence on time can be replaced by the monotonically increasing phase variable (normalized to be between 0 and 1).

biped and the stance hip,

$$\theta_{\text{P.V}} = tan^{-1}\left(\frac{-(l_1 sin(\theta_1) + l_2 sin(\theta_2))}{(l_1 cos(\theta_1) + l_2 cos(\theta_2))}\right) \quad (6)$$

where L_1 is the length of the shank link, l_2 is the length of the femur link, θ_1 is the angle of the shank link with respect to vertical, θ_2 is the angle of the femur link with respect to vertical. This phase variable is similar to work done in [13], as this angle was shown to increase monotonically throughout gait.

The use of virtual constraints as a means to create an autonomous control framework not only allows for stability to be guaranteed but this method also possesses more robust stability properties [23]. These robust stability properties stem from the fact that the system does not need to return to a particular instance in time following a perturbation, which occurs with time-dependent reference trajectories. Instead, the system can react to the perturbation, which would result in a change in the phase variable. From this change in the phase variable, the resultant reference trajectories would change accordingly, and the biped could continue tracking. This time-invariant phase variable provides disturbance handling that is similar to how humans handle perturbations related to gait [23].

IV. ASSISTANCE-AS-NEEDED CONTROL
Proper rehabilitation of gait for a stroke victim involves the promotion of brain plasticity [7]. One way in which a patient can achieve functional motor recovery following a neurological injury is to have a rehabilitation program that promotes high-intensity training [24]. AAN control increases the intensity of the rehabilitation by reducing the possibility for the patient to slack throughout the gait cycle. Reducing the possibility to slack is achieved by only providing corrective

torques if the patient deviates substantially from the desired joint angle trajectories.
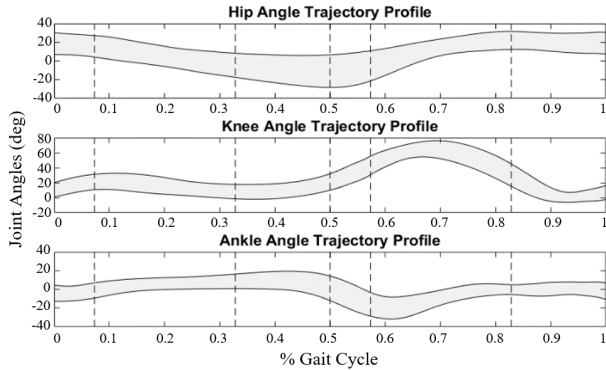

FIGURE 5. Joint angle reference trajectories are now tunnel trajectories in which the controller does no work if the tracking error is within the specified bounds. The specified bounds are related to the known standard deviation in human walking (1.25xSt.Dev).

AAN control was achieved by placing a deadzone around the desired reference trajectory of each of the actuated joints on the exoskeleton, originally developed in [25]. The deadzone illustrated in Figure 5 was chosen to be 1.25 times the standard deviation in typical human walking. Non-zero control torques are only applied if any of the joint angles trajectories deviate outside of their associated deadzone, as defined by the upper and lower thresholds,

$$\theta_{d,i} = \{\theta_{r,i}\,(\theta_{P.V}) + 1.25x\sigma_i,$$
$$\theta_{r,i}\,(\theta_{P.V}) + 1.25x\sigma_i \qquad (7)$$

where $\theta_{d,i}$ defines the bounds of the desired deadzone trajectory of each joint, σ_i is the standard deviation associated with each joint, originally developed in [25], and $\theta_{r,i}\,(\theta_{P.V})$ is the mean joint angle reference trajectory determined from the phase variable, $\theta_{P.V}$.

This deadzone size of 1.25 times the standard deviation in typical human walking was chosen as it led to adequate freedom around the desired trajectory without having the ability to deviate to the point that premature contact could be made with the ground, thus resulting in a fall. Typical human walking is known to be within two standard deviations of the desired trajectory. The chosen deadzone size, therefore, envelops trajectories that are always in the biomimetic range. Individual deadzones where placed around the actuated joints of the exoskeleton instead of around the end effector trajectory as this ensures biomimetic trajectories are enforced at each joint and not simply on the foot path.

V. VELOCITY MODULATED DEADZONE CONSTRAINT

Virtual constraints can be chosen to ensure stability when trajectories are explicitly enforced via feedback loops at the joint level [15]. However, when virtual constraints only activate outside of a deadzone, it becomes much harder to ensure stability. For deadzones large enough to be clinically relevant,

it is possible for sufficient momentum to be lost within the deadzone that the exoskeleton stops walking. Remember that virtual constraint control uses an autonomous control strategy, and thus has no explicit concept of time. Momentum loss must accordingly be constrained within the deadzone to ensure walking stability.

The key innovation of our work is to introduce a velocity-dependent restriction on the size of the deadzone, which ensures adequate momentum and thus gait stability. This restriction begins when the horizontal velocity of the biped drops below 1.1m/s. The deadzone size is reduced to zero when the horizontal linear velocity of the biped drops below 1m/s, at which point stability could no longer be guaranteed. The restriction occurs over a small change in horizontal walking speed to ensure the deadzone remains as large as possible while stability can be guaranteed. The deadzone size is restricted using a sigmoid function scaling factor,

$$S.F = -49492.4\frac{s^5}{m^5} * \left(|V_{CoMx}| - 1\frac{m}{s}\right)^5 - 951.777\frac{s^4}{m^4}$$
$$* \left(|V_{CoMx}| - 1\frac{m}{s}\right)^4 + 1840.1\frac{s^3}{m^3} * \left(|V_{CoMx}| - 1\frac{m}{s}\right)^3 \qquad (8)$$

where V_{CoMx} is the velocity of the CoM of the biped in the horizontal direction, and S.F is the scaling factor multiplied by the standard deviation of each joint angle trajectory ($0 \leq S.F \leq 1.25$). The sigmoid function ensures a smooth restriction occurs, rather than on on/off type modulation of the deadzone size. We use a minimum-jerk sigmoid function scaling, but any sigmoid function should be sufficient.

This deadzone modulation forces the controller to take a more active role following movements within the deadzone that cause a loss in walking speed below the specified threshold so that continued progression can be achieved throughout the gait cycle. Upon restoring momentum above the threshold, the controller then restores the deadzone around the desired trajectory so that the AAN policy can be achieved.

VI. RESULTS AND DISCUSSION

Simulations for a variety of different gait pathologies were performed in order to validate the proposed autonomous AAN control law (see Figure 6). These tested pathologies include full strength gait, paretic gait, hemiparetic gait, general weakness across all joints, drop foot, and unilateral weakness getting progressively worse from hip to ankle.

The proposed control law was robust enough to handle each pathology and facilitate stable steady state walking without knowledge of the individual pathologies. For the purpose of this paper, however, the results for paretic gait and hemiparetic gait are included.

A. COMPLETE LOWER LIMB PARALYSIS SIMULATION

Analyzing the joint angle trajectory outputs for the paretic simulation show that the controller achieves biomimetic gait patterns (see Figure 7). For the stride depicted in the results, no modulation of the deadzone size was required as there
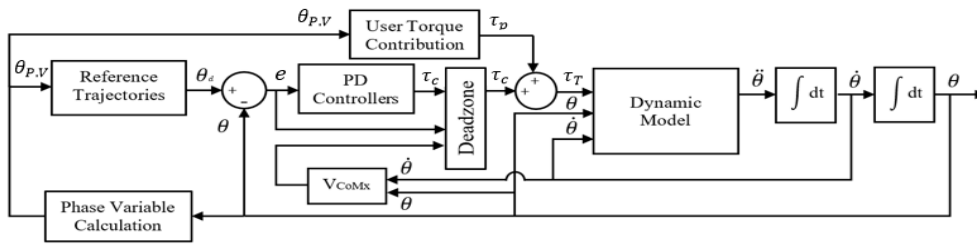
FIGURE 6. Block diagram of the AAN controller with the user torque contribution for different gait pathologies. The dynamic model block contains the dynamics associated with each of the three previously described sub phases. The deadzone block applies the control torques to the dynamic model if the tracking error (e) is greater than the 1.25xSt.Deviation threshold for any of the joints.
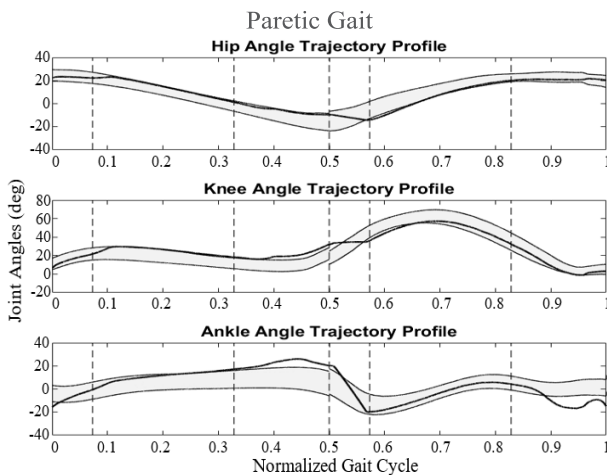

FIGURE 7. Joint angle trajectory plots, for paretic gait, show that the controller was able to maintain biomimetic walking profiles by forcing the trajectories back into the deadzone throughout gait.
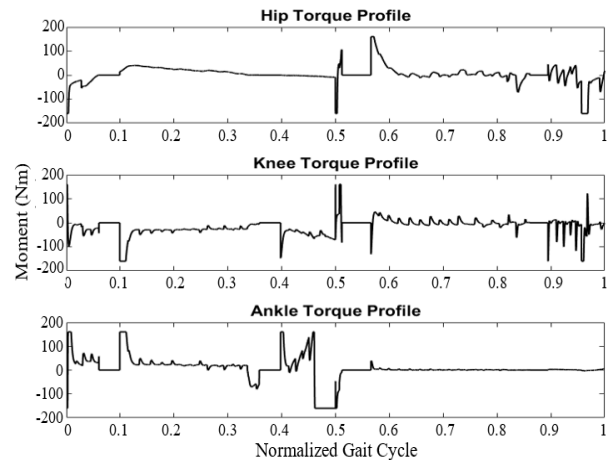

FIGURE 8. Control torques for each joint, given the paretic gait, show areas of zero torque when each of the joints is within the specified deadzone.

was no reduction in walking speed below the 1m/s threshold. Therefore, the size of the deadzones remained at the 1.25 times standard deviation limit for the full gait cycle. Had a loss in walking speed been observed, the deadzone sizes would have been restricted to ensure the controller takes over the actuation of each joint. The proposed control strategy only applies corrective torques if one of the joints deviates outside of the deadzone. It can be seen by analyzing the control torques associated with the paretic gait simulation that there are areas of zero control torque at the start of both the stance and swing phases of gait (see Figure 8). The controller was only able to briefly apply zero control torque as the simulated patient had zero retained strength and quickly began to fall outside of the deadzone.

B. HEMIPARETIC GAIT SIMULATION
The joint angle trajectory outputs associated with the hemiparetic gait simulation show that the proposed control framework was able to achieve biomimetic gait trajectories (see Figure 9). Comparing the hemiparetic control torque outputs to those from the full paretic simulation shows that there is an increase in the number of times when the controller outputs are zero. Increases in zero control torque are

especially evident in the swing phase of gait (see Figure 10). These increases in areas of zero control torque are due to the increase in retained strength in the hemiparetic gait simulation. Therefore, the controller is allowing the patient to complete that section of gait as they are able to stay within the bounds of normal human walking more often.

Similar conclusions can be drawn by looking at the joint angle trajectory outputs. When analyzing the outputs from the full paretic gait, it was noted that the trajectory outputs approach the upper and lower bounds of normal walking very quickly as the simulated patient is not able to provide any joint torques. The hemiparetic outputs at the knee and hip joint show that there are fewer harsh approaches to the bounds of the tunnel trajectory, especially in the swing phase of gait. This ability to naturally stay within the bounds of the deadzone also explains why there were more areas of zero control torque during this phase when comparing the two simulations. The patient is able to contribute more towards the completion of their gait and therefore, the controller does no work.

There are a few areas in which the desired control policy was not able to maintain the trajectories within the specified deadzone. These areas are mainly in the underactuated phase
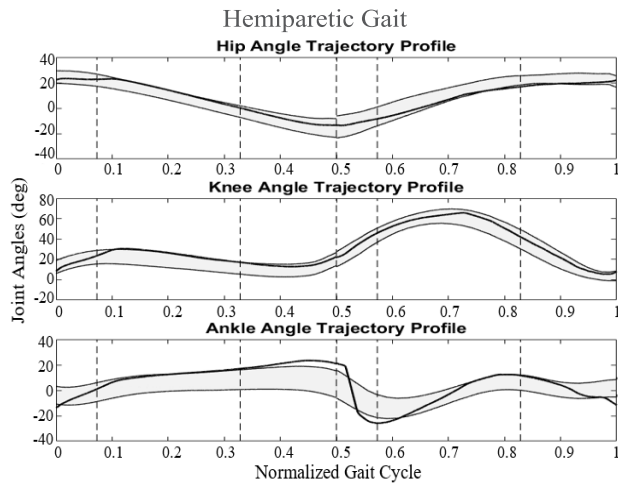
FIGURE 9. Joint angle trajectory plots of the leg with no retained strength, for hemiparetic gait, show that the controller was able to maintain biomimetic walking profiles by forcing the trajectories back into the deadzone throughout gait.
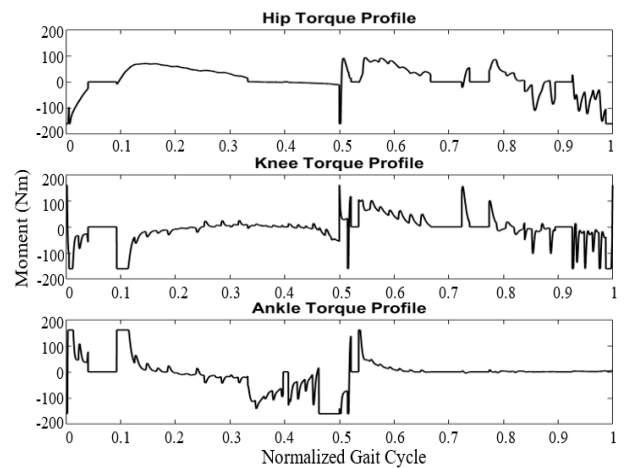

FIGURE 10. Control torques for each joint of the leg with no retained strength, in the hemiparetic simulation, shows areas of zero torque when each of the joints is within the specified deadzone.

between 40-50% and between 90-100% of the gait cycle. This lack of containment within the deadzone stems from how the joint angles were referenced. The joint angles in this model were referenced with respect to vertical rather than using relative joint angle references.

Therefore, when the model is in the underactuated phase of gait there is no way to acquire information about the relative joint angle between the stance shank and stance foot. Furthermore, because a desired trajectory cannot be tracked at the toe during underactuation this leads to tracking discrepancies when trying to stay within the deadzone, especially at the ankle joint. Also, near the end of the joint angle trajectories at 100% of the gait cycle contact is made with the ground thus forcing the swing foot flat which leads to the ankle trajectory deviating outside of the deadzone as well.

The AAN control policy presented in this work provides theoretical improvements to current adaptive AAN policies used to rehabilitate lower limb gait pathologies. The proposed AAN control strategy was applied to a 6DOF lower limb exoskeleton whereas the work done in [12] applies an adaptive AAN control policy to a single limb while ambulating on a treadmill. Providing actuation to both legs allows for the device to be used to rehabilitate patients that do not simply have a unilateral gait pathology. Furthermore, deadzones were placed at each joint of the exoskeleton device instead of at the end effector position, thus ensuring biomimicry is achieved at the joint level. Also, in this work stability is formally analyzed, in contrast to more anecdotal proof in other work (e.g. the work done in [12]).

C. STABILITY ANALYSIS

With the implementation of the autonomous control strategy as a means to facilitate gait rehabilitation, the stability of the system can now be formally demonstrated. In this work

we approach stability within a state-space framework [26], broadly defining it by the ability of the controller to remain within the vicinity of a bounded invariant set in terms of positional and velocity state information. For continuously differentiable systems, state-state stability benefits from the formalism of stability in the sense of Lyapunov. For hybrid systems such as periodic orbits in bipedal walking, Poincare mappings are typically used instead to determine the existence and assess the stability of periodic orbits in bipedal walking [27], [28]. In this work, however, the bipedal walking is aperiodic given the allowance for state and time variations throughout gait, due to the autonomous control framework as well as the deadzone around the joint angle trajectories. Lorenz mappings are a useful tool to analyze the stability of aperiodic systems, by looking at the maximum or minimum value of a particular metric at any point in the gait cycle, rather than at a specific instance in the state flow like Poincare mappings [29]. Lorenz mappings can both demonstrate state boundedness and show the relationship between deadzone size and the boundaries of the chaotic behaviour.

In the analysis of this bipedal system, two different metrics were used in order to draw conclusions about the systems overall stability. The first metric was step length. Maintaining consistent step lengths throughout steady-state walking means that proper progression of the phase variable is achieved. Therefore, proper tracking of each actuated joint is also achieved given the adequate PD gains of the control law. The second metric used for the stability analysis was the horizontal velocity of the CoM of the bipedal system. If the analysis shows that the walking speed is maintained, then this means that the phase variable is progressing at the correct rate as well. Having information regarding each of the positional and velocity states means one can draw conclusions regarding the systems overall stability.

The first pathology that was analyzed using the previously described stability analysis technique was the full paretic gait in which the patient is unable to contribute any effort in their lower limbs. Looking at the Lorenz maps associated with the
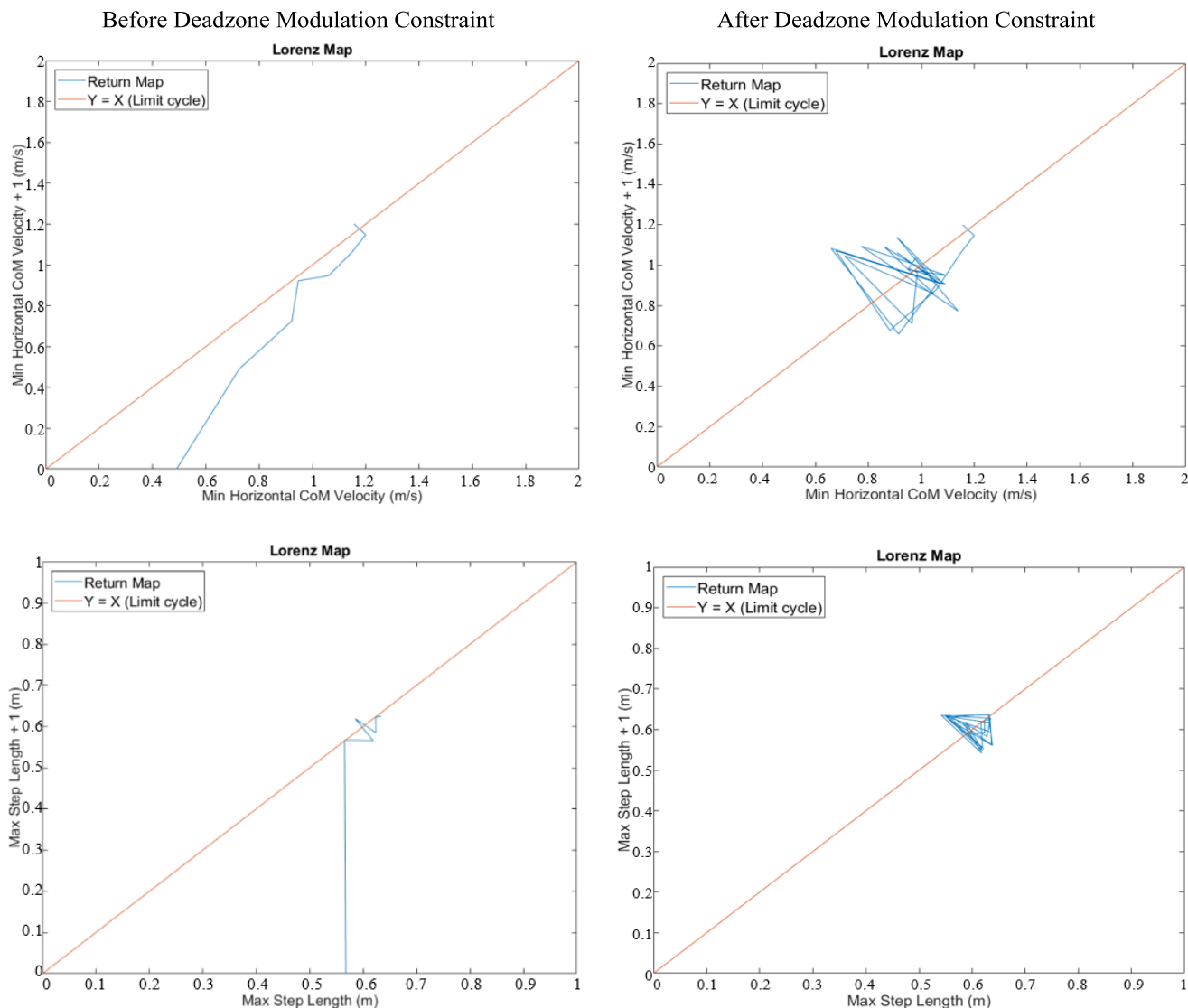
Before Deadzone Modulation Constraint

After Deadzone Modulation Constraint

FIGURE 11. Lorenz maps of minimum horizontal CoM velocity and max step length. The results show that the deadzone modulation constraint was able to stabilize walking when previously a loss in momentum was observed.

velocity of the CoM and the step length before the deadzone modulation constraint (see Figure 11) it can be seen that unstable walking was produced as both maps collapse to zero on the y-axis. This collapse to zero on the y-axis means that the control law was unable to maintain walking momentum, despite using virtual constraint control, due to the presence of the deadzone.

After the velocity dependant deadzone modulation constraint, it can be seen that the control law was able to correct for the decrease in walking speed. The Lorenz map still shows fairly chaotic behaviour around the line y = x, relating to a limit cycle, as the patient is continuously losing momentum given their lack of any retained strength and the allowance for motion within the deadzone. Due to the fact that they have no retained strength, they are unable to ensure the proper progression of the phase variable is achieved and therefore,

the constraint must force a collapse in the deadzones and take control of the walking until the walking speed increases above the threshold. Analyzing the Lorenz map of the step length achieved throughout steady-state walking after the implementation of the constraint, it is clear that the controller was able to produce consistent step lengths. The small amount of deviation around the line y = x is due to the allowable joint angle deviations within the deadzone, thus producing slightly different step lengths throughout the simulation.

The second pathology that was analyzed using the concept of Lorenz mapping was the simulated hemiparetic gait pathology. This pathology relates to the patient having full strength in one of their limbs but having no retained strength in the other limb. This pathology is common following a stroke and must be tested using the proposed rehabilitative control law as stroke rehabilitation is the main focus of this work.
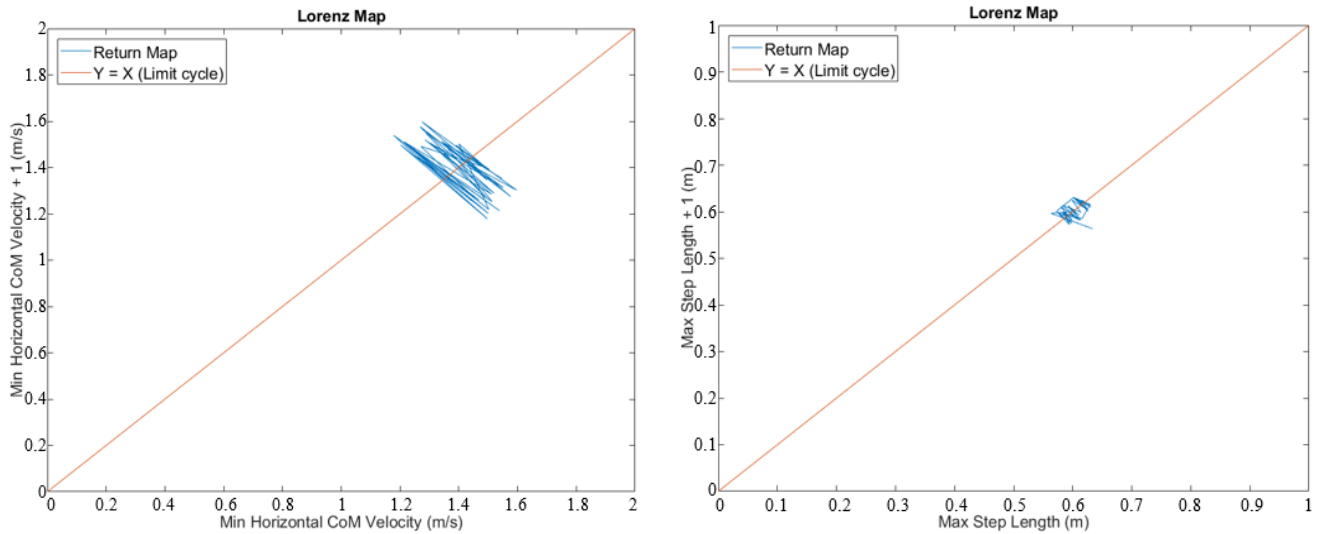
FIGURE 12. The Lorenz maps for minimum horizontal walking speed and maximum step length. The results show that the controller was able to maintain a steady state walking speed and produce consistent step lengths for a simulated patient with hemiparesis.
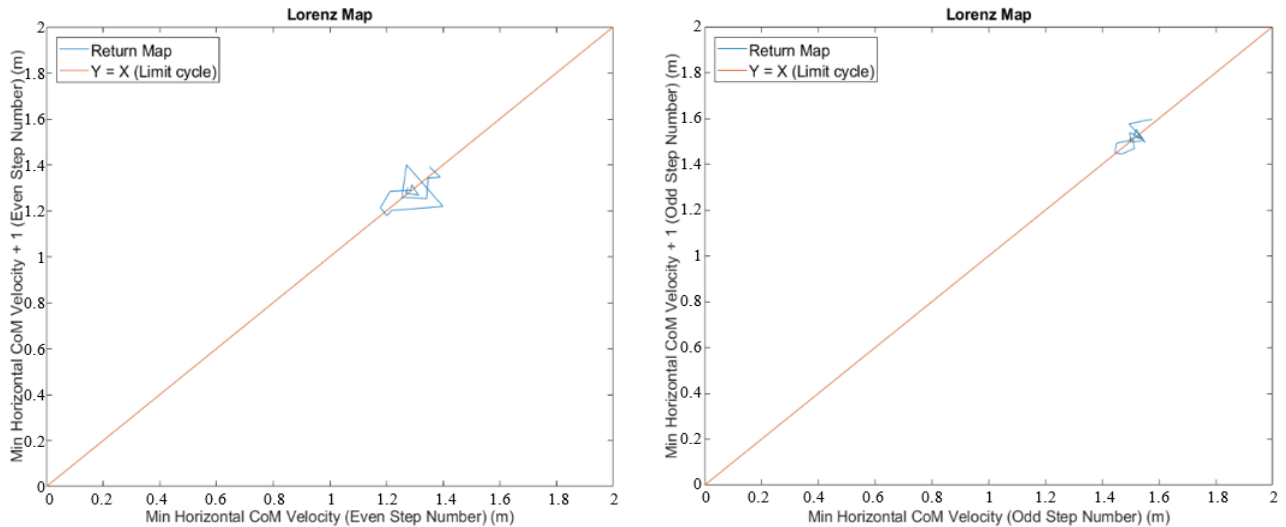

FIGURE 13. Lorenz maps created for every second step. Using Lorenz maps to analyze the behaviour of the system every second step, for the minimum horizontal CoM velocity metric, it is noticed that the chaotic behaviour is reduced, and the system more tightly approaches a limit cycle. This behaviour leads to the observation that second order periodicities are present given the unilateral gait pathology.

Analyzing the Lorenz maps associated with the hemiparetic gait simulation (see Figure 12) it can be seen that an appropriate steady-state walking speed was achieved using the proposed velocity-modulated control law. Adequate steady-state walking was achieved as there are no deviations towards infinity, nor are there any indications that the bipedal model was losing momentum and slowing down towards zero. Also, by looking at the Lorenz map associated with the step length it can be seen that appropriate step lengths were achieved throughout the steady-state walking simulation. Similar to the paretic gait pathology simulation, the hemiparetic simulation led to small variations in the step

length due to the allowable deviations of each joint within their respective deadzone.

It is interesting to note that these two different pathologies resulted in different walking speeds as the patient has some control over the speed in which the phase variable progresses. In the paretic pathology simulation, the average walking speed was around 1m/s whereas for the hemiparetic gait pathology the average walking speed was around 1.4m/s. This difference in walking speed stems from the fact that the patient's effort is actively considered throughout gait and therefore, they have the ability to chose how fast the phase variable progresses if they have enough retained strength.

Throughout this work it is interesting that the walking speed for the hemiparetic gait seems fairly chaotic given the jumping across the line y = x on the Lorenz map. If instead the Lorenz map is split into two separate maps; one for the right leg as the stance leg and the other for the left leg as the stance leg an increase in the collapse around the line y = x is achieved (see Figure 13). This decrease in chaotic behaviour when looking at every second step shows that second-order periodicies are present given the unilateral gait pathology. These second-order periodicies mean that the controller was able to more closely replicate the gait pattern when the paretic leg was used as the stance leg. Also, a different but still repeatable gait pattern was achieved when the unimpaired limb was used as the stance leg. This difference in gait stems from the fact the controller is able to apply zero torque more when one limb is being used as the stance leg versus when the other limb is being used as the stance leg given the discrepancies in weakness between the two limbs with the tested hemiparetic pathology.

VII. CONCLUSION

This paper details the implementation of an autonomous assistance-as-needed control law that facilitates walking rehabilitation for a variety of gait pathologies commonly found following a stroke. The simulation results of the proposed control law show that there is a consideration of the patient's retained strength in real-time with no patient-specific tuning required, thus further promoting brain plasticity. This consideration of retained strength is shown by the allowable joint angle deviations within the deadzone as well as the periods of zero control torque throughout walking. Furthermore, this control strategy provides improvements to previous rehabilitative exoskeletons as the autonomous control framework allows for a variety of walking speeds to be achieved in real-time. This ability to self-select a walking speed if the patient has sufficient retained strength further promotes brain plasticity and adds another dimension of complexity to the rehabilitation program.

Assistance-as-needed control was achieved by placing a deadzone around each of the desired joint angle trajectories to ensure biomimetic walking profiles could be performed without controller interference. Given the size of the deadzones around the desired trajectories, motions within the deadzone could result in a loss in momentum given that the controller has no explicit concept of time. A velocity dependant modulation constraint was created to ensure the controller enforced more strict tracking following motions that caused a loss in momentum, to ensure steady state walking was maintained.

The stability of the proposed control law was demonstrated when the exoskeleton system maintained a bounded walking speed and a bounded step length, illustrated using Lorenz mappings. The use of Lorenz mappings allowed for state boundedness to be demonstrated given the contained motion around the line y = x. This analysis method differs from the classical bipedal walking analysis method of Poincare mapping as walking is no longer periodic. The exoskeletons

stability is guaranteed given the autonomous control framework and therefore, does not require the use of external stability aids and can be used at a variety of different walking speeds.

In future work, the proposed control policy could be implemented on a rehabilitation exoskeleton and tested on patients who have had a stroke as this would further confirm the ability of the controller to facilitate gait rehabilitation. Also, the control law could be further refined to reduce control chattering at the boundary layer of the deadzone. Achieving this reduction in control chattering could be done by adding control interpolation at the boundary layer, similar to the implementation of reduced control chattering in a sliding mode controller. Finally, increased robustness testing could be performed with respect to measurement noise as well as modelling uncertainty.

REFERENCES

[1] *World Health Report*, Geneva, Switzerland, World Health Org., 2002.
[2] T. Yan, M. Cempini, C. M. Oddo, and N. Vitiello, "Review of assistive strategies in powered lower-limb orthoses and exoskeletons," *Robot. Auto. Syst.*, vol. 64, pp. 120–136, Feb. 2015.
[3] M. Talaty, A. Esquenazi, and J. E. Briceno, "Differentiating ability in users of the ReWalk powered exoskeleton: An analysis of walking kinematics," in *Proc. IEEE 13th Int. Conf. Rehabil. Robot. (ICORR)*, Jun. 2013, pp. 1–5.
[4] R. J. Farris, H. A. Quintero, S. A. Murray, K. H. Ha, C. Hartigan, and M. Goldfarb, "A preliminary assessment of legged mobility provided by a lower limb exoskeleton for persons with paraplegia," *IEEE Trans. Neural Syst. Rehabil. Eng.*, vol. 22, no. 3, pp. 482–490, May 2014.
[5] A. Agrawal, O. Harib, A. Hereid, S. Finet, M. Masselin, L. Praly, A. D. Ames, K. Sreenath, and J. W. Grizzle, "First steps towards translating HZD control of bipedal robots to decentralized control of exoskeletons," *IEEE Access*, vol. 5, pp. 9919–9934, 2017.
[6] L. Marchal-Crespo and D. J. Reinkensmeyer, "Review of control strategies for robotic movement training after neurologic injury," *J. Neuroeng. Rehabil.*, vol. 6, no. 20, Jun. 2009, doi: 10.1186/1743-0003-6-20.
[7] M. S. Burns, "Application of neuroscience to technology in stroke rehabilitation," *Topics Stroke Rehabil.*, vol. 15, no. 6, pp. 570–579, Nov. 2008.
[8] R. Riener, L. Lunenburger, S. Jezernik, M. Anderschitz, G. Colombo, and V. Dietz, "Patient-cooperative strategies for robot-aided treadmill training: First experimental results," *IEEE Trans. Neural Syst. Rehabil. Eng.*, vol. 13, no. 3, pp. 380–394, Sep. 2005.
[9] eksobionics. *Exoskeletons for Medical and Industrial Uses*. Accessed: Jul. 2, 2019. [Online]. Available: https://eksobionics.com/
[10] M. Bortole, "The H2 robotic exoskeleton for gait rehabilitation after stroke: Early findings from a clinical study," *J. Neuroeng. Rehabil.*, vol. 12, no. 54, Jun. 2015, doi: 10.1186/s12984-015-0048-y.
[11] S. A. Murray, K. H. Ha, and M. Goldfarb, "An assistive controller for a lower-limb exoskeleton for rehabilitation after stroke, and preliminary assessment thereof," in *Proc. 36th Annu. Int. Conf. IEEE Eng. Med. Biol. Soc.*, Aug. 2014, pp. 4083–4086.
[12] S. K. Banala, S. K. Agrawal, and J. P. Scholz, "Active leg exoskeleton (ALEX) for gait rehabilitation of motor-impaired patients," in *Proc. IEEE 10th Int. Conf. Rehabil. Robot.*, Jun. 2007, pp. 401–407.
[13] C. Chevallereau, G. Abba, Y. Aoustin, F. Plestan, E. R. Westervelt, and C. Canudas-de-Wit, "RABBIT: A testbed for advanced control theory," *IEEE Control Syst. Mag.*, vol. 23, no. 5, pp. 57–79, Oct. 2003.
[14] E. R. Westervelt, J. W. Grizzle, C. Chevallereau, J. H. Choi, and B. Morris, *Feedback Control of Dynamic Bipedal Robot Locomotion*. Boca Rato, FL, USA: Taylor & Francis, 2007.
[15] R. D. Gregg, T. Lenzi, L. J. Hargrove, and J. W. Sensinger, "Virtual constraint control of a powered prosthetic leg: From simulation to experiments with transfemoral amputees," *IEEE Trans. Robot.*, vol. 30, no. 6, pp. 1455–1471, Dec. 2014.
[16] X. Mu, "Dynamics and motion regulation of a five-linked biped robot walking in the sagittal plane," Ph.D. dissertation, Univ. Manitoba, Winnipeg, MB, Canada, 2005.

[17] M. P. Mcgrath, "Appropriately complex modelling of healthy human walking," Ph.D. dissertation, Univ. Salford, Salford, U.K., Jun. 2014.

[18] C. Chevallereau, A. Formal'sky, and B. Perrin, "Low energy cost reference trajectories for a biped robot," in *Proc. IEEE Int. Conf. Robot. Autom.*, Nov. 2002, pp. 1398–1404.

[19] J. Furusho and M. Masubuchi, "Control of a dynamical biped locomotion system for steady walking," *J. Dyn. Syst., Meas., Control*, vol. 108, no. 2, pp. 111–118, Jun. 1986.

[20] M. Garcia, A. Chatterjee, A. Ruina, and M. Coleman, "The simplest walking model: Stability, complexity, and scaling," *J. Biomech. Eng.*, vol. 120, no. 2, pp. 281–288, Apr. 1998.

[21] H. Hemami and R. Farnsworth, "Postural and gait stability of a planar five link biped by simulation," *IEEE Trans. Autom. Control*, vol. AC-22, no. 3, pp. 452–458, Jun. 1977.

[22] A. Mohammadi, M. Maggiore, and L. Consolini, "Dynamic virtual holonomic constraints for stabilization of closed orbits in underactuated mechanical systems," *Automatica*, vol. 94, pp. 112–124, Aug. 2018.

[23] R. D. Gregg, E. J. Rouse, L. J. Hargrove, and J. W. Sensinger, "Evidence for a time-invariant phase variable in human ankle control," *PLoS ONE*, vol. 9, no. 2, Feb. 2014, Art. no. e89163.

[24] P. Langhorne, J. Bernhardt, and G. Kwakkel, "Stroke rehabilitation," *Lancet*, vol. 377, no. 9778, pp. 1693–1702, May 2011.

[25] D. A. Winter, "Biomechanics of human movement," in *Illustrate*. Hoboken, NJ, USA: Wiley, 1979.

[26] K. Hassan, *Nonlinear Systems*, 3rd ed. Upper Saddle River, NJ, USA: Prentice-Hall, 2002.

[27] Y. Hurmuzlu and C. Basdogan, "On the measurement of dynamic stability of human locomotion," *J. Biomech. Eng.*, vol. 116, no. 1, pp. 30–36, Feb. 1994.

[28] B. Morris and J. W. Grizzle, "A restricted Poincaré map for determining exponentially stable periodic orbits in systems with impulse effects: Application to bipedal robots," in *Proc. 44th IEEE Conf. Decis. Control*, Oct. 2006, pp. 4199–4206.

[29] E. N. Lorenz, "Deterministic nonperiodic flow," *J. Atmos. Sci.*, vol. 20, no. 2, pp. 130–141, 1963.

CHRIS P. DIDUCH (Senior Member, IEEE) received the Ph.D. degree in the area of advanced controls from the University of New Brunswick (UNB), Fredericton, NB, Canada, in 1986. He currently serves as the Dean of the Faculty of Engineering, UNB, and as the Acting Director of the Emera and NB Power Research Centre for Smart Grid Technologies. His research interests include application of advanced estimation, detection and control theory in power electronic converters, aggregated control of distributed energy resources in electric power systems, and robotics. He is a member of the Association of Professional Engineers and Geoscientists of New Brunswick.

SAMUEL M. CAMPBELL received the B.Sc. degree in mechanical engineering from the University of New Brunswick, Fredericton, NB, Canada, in 2017, where he is currently pursuing the M.Sc. degree in electrical engineering. His research interests include exoskeleton design and control, as well as robotic gait modeling and simulation.

JONATHON W. SENSINGER (Senior Member, IEEE) received the B.S. degree in bioengineering from the University of Illinois at Chicago, Chicago, IL, USA, in 2002, and the Ph.D. degree in biomedical engineering from Northwestern University, Chicago, in 2007. He is the Director of the Institute of Biomedical Engineering, University of New Brunswick, Fredericton, NB, Canada, where he is also a Professor of electrical and computer engineering. His research interests include prosthesis and exoskeleton design, control, sensory feedback, and outcome measures. His current research focuses on human–machine interfaces using haptics and computational motor control approaches. He is a member of the Association of Professional Engineers and Geoscientists of New Brunswick.

• • •